1-1-2017

Flexural behaviour of GFRP reinforced high strength and ultra high strength concrete beams

Matthew Goldston
University of Wollongong, mwg278@uowmail.edu.au

Alex M. Remennikov
University of Wollongong, alexrem@uow.edu.au

M Neaz Sheikh
University of Wollongong, msheikh@uow.edu.au

Flexural behaviour of GFRP reinforced high strength and ultra high strength concrete beams

Abstract

FRP bars are considered alternatives to steel bars for reinforcing concrete structures in harsh environments. FRP bars are non-corrosive, light weight, non-magnetic and have high longitudinal strength and low thermal and electric conductivity. This paper experimentally investigated the flexural behaviour of high strength concrete (HSC) and ultra-high strength concrete (UHSC) beams reinforced with glass fiber reinforced polymer (GFRP) bars that has not been addressed in the literature before. Beams of 2400 mm long, 100 mm wide and 150 mm high were tested under quasi-static loading (three point loading). Influence of reinforcement ratio and compressive strength of concrete (HSC and UHSC) on the load carrying capacity, deflection, energy absorption, strains in the concrete and reinforcement, and failure modes were investigated. Test results found that over-reinforced HSC and UHSC GFRP bar reinforced concrete (GFRP-RC) beams showed an amount of pseudo ¿ductility¿ compared to under-reinforced HSC and UHSC GFRP-RC beams, where failure was brittle, without any prior warning. Energy absorption capacities were found to be higher for UHSC GFRP-RC beams for the same amount of reinforcement compared to HSC GFRP-RC beams. FRP design recommendations in ACI (2015) and CSA (2012) were compared with experimental data. FRP design recommendations for the calculation of flexural strength were found to be conservative (load-carrying capacity was under-predicted by 36% for both HSC GFRP-RC beams and UHSC GFRP-RC beams). However, FRP design recommendations for the calculation of deflection at the load carrying capacity were found to be un-conservative (deflections were under-predicted by an average of 10-22% for the HSC GFRP-RC beams and UHSC GFRP-RC beams).

Disciplines

Engineering | Science and Technology Studies

Publication Details

Goldston, M. W., Remennikov, A. & Sheikh, M. (2017). Flexural behaviour of GFRP reinforced high strength and ultra high strength concrete beams. Construction and Building Materials, 131 606-617.

FLEXURAL BEHAVIOUR OF GFRP REINFORCED HIGH STRENGTH AND ULTRA HIGH STRENGTH CONCRETE BEAMS

M.W.Goldston[1], A. Remennikov[2,*] and M. Neaz Sheikh[3]

Affiliation:

[1]Postgraduate Research Student, School of Civil, Mining and Environmental Engineering, University of Wollongong, Australia

[2]Associate Professor, School of Civil, Mining and Environmental Engineering, University of Wollongong, Australia

[3]Senior Lecturer, School of Civil, Mining and Environmental Engineering, University of Wollongong, Australia

Correspondence:

Name: A. Remennikov

Address: School of Civil, Mining and Environmental Engineering

University of Wollongong

Northfields Avenue, Wollongong NSW 2522

E-mail: alexrem@uow.edu.au

Telephone: 61 2 4221 5574

---

* Corresponding authors

Research Highlights

- HSC and UHSC GFRP-RC beams reinforced with GFRP bar were tested to investigate flexural behaviour
- Failure modes of HSC and UHSC GFRP-RC beams were identified.
- FRP design recommendations were compared with experimental results.
- Over-reinforced HSC and UHSC GFRP-RC beams showed an amount of pseudo "ductility".

FLEXURAL BEHAVIOUR OF GFRP REINFORCED HIGH STRENGTH AND ULTRA HIGH STRENGTH CONCRETE BEAMS

M.W.Goldston[1], A. Remennikov[2] and M. Neaz Sheikh[3]

[1]Postgraduate Student, School of Civil, Mining and Environmental Engineering, University of Wollongong, Australia

[2]Associate Professor, School of Civil, Mining and Environmental Engineering, University of Wollongong, Australia

[3]Senior Lecturer, School of Civil, Mining and Environmental Engineering, University of Wollongong, Australia

ABSTRACT

FRP bars are considered alternatives to steel bars for reinforcing concrete structures in harsh environments. FRP bars are non-corrosive, light weight, non-magnetic and have high longitudinal strength and low thermal and electric conductivity. This paper experimentally investigated the flexural behaviour of high strength concrete (HSC) and ultra-high strength concrete (UHSC) beams reinforced with glass fiber reinforced polymer (GFRP) bars that has not been addressed in the literature before. Beams of 2400 mm long, 100 mm wide and 150 mm high were tested under quasi-static loading (three point loading). Influence of reinforcement ratio and compressive strength of concrete (HSC and UHSC) on the load carrying capacity, deflection, energy absorption, strains in the concrete and reinforcement, and failure modes were investigated. Test results found that over-reinforced HSC and UHSC GFRP bar reinforced concrete (GFRP-RC) beams showed an amount of pseudo “ductility” compared to under-

reinforced HSC and UHSC GFRP-RC beams, where failure was brittle, without any prior warning. Energy absorption capacities were found to be higher for UHSC GFRP RC beams for the same amount of reinforcement compared to HSC GFRP RC beams. FRP design recommendations in ACI (2015) and CSA (2012) were compared with experimental data. FRP design recommendations for the calculation of flexural strength were found to be conservative (load-carrying capacity was under-predicted by 36% for HSC GFRP RC beams and UHSC GFRP RC beams). However, FRP design recommendations for the calculation of deflection at ultimate load were found to be un-conservative (deflections were under-predicted by an average of 10-22% for HSC GFRP RC beams and UHSC GFRP RC beams).

Keywords: GFRP bar, RC beam, HSC, UHSC, Deflection, Flexure, Energy Absorption.

1. Introduction

Steel bars have been traditionally used as reinforcement for concrete structures. However, the use of steel bars is not recommended in marine and coastal areas [1]. This is due to the possibility of corrosion of the reinforcing steel in the concrete structures [2], causing structural, financial and safety concerns. To prevent corrosion, the use of Fibre-Reinforced Polymer (FRP) bars is recommended in aggressive environments [3]. Advantages of FRP bars over conventional steel bars include non-corrosive behaviour, high longitudinal tensile strength in the direction of the fibres, non-magnetic and lightweight characteristics. However, FRP bars are brittle with linear-elastic stress-strain behaviour. FRP bars do not yield like steel reinforcement. Other disadvantages of FRP bars include low elastic modulus, low shear strength and high cost. However, the use of FRP bars to reinforce marine infrastructure, where corrosion of steel is highly likely, the service life and durability of the marine structures will be increased, resulting

96 in a decrease in overall life-cycle costs [4]. Available FRP bars for commercial use include glass
97 FRP bars (GFRP), carbon FRP (CFRP), aramid FRP (AFRP) and basalt FRP (BFRP). These
98 types of FRP bars have varying mechanical and physical properties as well as different surface
99 configurations.

100 The flexural behaviour of FRP-reinforced concrete (FRP-RC) beams has been extensively
101 studied [4-14]. In these studies, the effects of normal and high strength concrete on the flexural
102 behaviour of FRP-RC beams were investigated. Majority of the previous studies investigated
103 beams with concrete strengths ranging from 20-80 MPa [4-12, 14]. However, there are only a
104 limited number of studies that investigated the flexural behaviour of FRP-RC beams with
105 concrete strengths greater than 80 MPa [13]. Faza and GangaRao [15] investigated the flexural
106 behaviour of GFRP-RC beams and reported that the use of higher strength concrete was
107 fundamental to exploit the high tensile strength of the GFRP reinforcement bars. Also, Nanni
108 [16] found that the flexural strength of beams reinforced with FRP bars was highly sensitive to
109 the compressive strength of the concrete and recommended that FRP bars be used with high
110 strength concrete. Similarly, Kalpana and Subramanian [12] stated that the use of high strength
111 concrete results in better performance of the GFRP-RC beams in terms of load carrying capacity
112 and mid-span deflection. Yost and Gross [17] reported that the use of higher strength concrete
113 resulted in more efficient use of the FRP reinforcement. Theriault and Benmokrane [13] reported
114 that the increase or the change in concrete strength did not affect the stiffness of the FRP-RC
115 beams. However, FRP-RC beams reinforced with larger amounts of reinforcement showed larger
116 stiffness compared to beams reinforced with less amount of longitudinal reinforcement.
117 Moreover, as concrete strength and reinforcement ratio increased, ultimate moment capacity
118 increased. Getzlaf [18] stated that for over-reinforced GFRP-RC beams, increasing the concrete

strength is most beneficial when higher amounts of reinforcement are used. Finally, Goldston et al. [4] reported that the use of higher strength concrete was most beneficial at controlling mid-span deflection as well as increasing bending stiffness. However, in contrast to Theriault and Benmokrane [13], concrete strength did not influence load carrying capacity of GFRP-RC beams in Goldston et al. [4]. Extensive research has been conducted into the flexural behaviour of FRP-RC beams constructed mostly with normal and to a limited extent with high strength concrete (< 100 MPa). However, no studies yet investigated the flexural behaviour of GFRP-RC beams with concrete strength greater than 100 MPa.

To address this issue, this paper presents the flexural behaviour of six GFRP-RC beams constructed with concrete of nominal compressive strengths of 80 MPa (high strength concrete, HSC) and 120 MPa (ultra-high strength concrete, UHSC). It is noted that concrete strength above 100 MPa has been defined as UHSC in Vincent and Ozbakkalogu [19] and Ozbakkalogu [20]. Experimental test results were also compared with FRP-RC beam design recommendations in ACI [21] and CSA [22]. It should be noted that the design recommendations in CSA [22] are applicable for concrete strengths up to 80 MPa. While in ACI [21], no limitations of concrete strength has been specified, although the stress block parameters reach the limiting value at concrete compressive strength of 56 MPa. Thus, the experimental results were used to investigate the applicability of the FRP design recommendations in ACI [21] and CSA [22] for concrete strengths greater than 80 MPa.

2. Experimental Program

2.1 Materials

Test specimens were batched onsite using concrete mix designs (Table 1) with nominal 28-day concrete compressive strengths of 80 and 120 MPa. Concrete compressive strengths were measured using three concrete cylinders each with 100 mm diameter and 150 mm height according to AS 1012.9 [23]. On the day of testing, the average compressive strength of concrete was found to be 95 MPa (for 80 MPa nominal concrete compressive strength) and 117 MPa (for 120 MPa nominal concrete compressive strength). Three different diameter GFRP bars were used as longitudinal reinforcement. GFRP bars were designated as #2 (nominal diameter of 6.35 mm), #3 (nominal diameter of 9.53 mm) and #4 (nominal diameter of 12.7 mm). All GFRP reinforcement bars were sand coated for increasing bond strength with the surrounding concrete. The GFRP bars were supplied by V-Rod Australia [24]. Three specimens of each diameter were tested for tensile properties including tensile strength, elastic modulus and rupture strain according to ASTM D7205/D7205M [25]. Tensile strength and elastic modulus were calculated using nominal diameters. Tensile properties of GFRP reinforcement bars are reported in Table 2. Fig. 1 shows the stress-strain behaviour of the tested GFRP reinforcement bars. Plain mild steel bar with a diameter of 4 mm was used as transverse reinforcement. Three specimens of plain steel bar were tested according to ASTM A370-14 [26]. The average yield strength and elastic modulus were found as 583 MPa and 158 GPa, respectively.

164

165 **Table 1.** Concrete Mix Designs

Material	Nominal Concrete Strength	
	80 MPa	**120 MPa**
Bastion General Purpose Cement	540 kg/m^3	600 kg/m^3
Fine Grade Fly Ash	40 kg/m^3	*
Micro Silica Densified Silica Fume	40 kg/m^3	40 kg/m^3
10 mm Aggregate	1040 kg/m^3	1020 kg/m^3
Coarse Sand	420 kg/m^3	450 kg/m^3
Fine Sand	100 kg/m^3	150 kg/m^3
Sika Viscocrete PC HRF2 (Superplasticiser)	4 L/m^3	5 L/m^3
Water	160 L/m^3	155m^3

166 Note: * = Not required for 120 MPa concrete

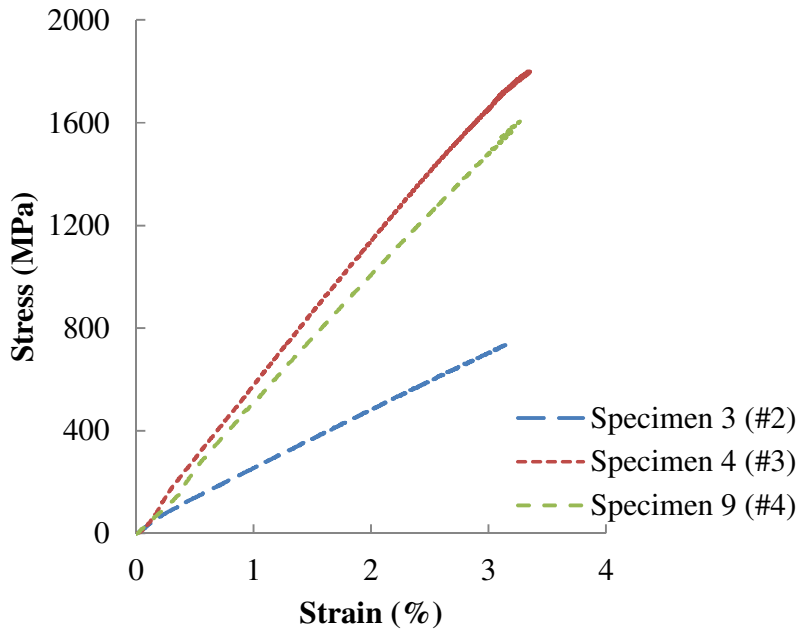

167

168 **Fig. 1**. Stress-Strain Curve of GFRP Tensile Test Specimens

169 **Table 2.** Tensile Test Results of GFRP Reinforcement Bars

Specimen (Designation)	Diameter, ∅ (mm)	L_a (mm)	L (mm)	L_{tot} (mm)	f_u (MPa)	ε_{fu} (%)	E_f (GPa)
1 (#2)	6.35	150	380	680	740	1.93	38.3
2 (#2)	6.35	150	380	680	718	1.94	37.1
3 (#2)	6.35	150	380	680	739	2.00	37.0
Mean					732	1.96	37.5
4 (#3)	9.53	400	200	1000	1801	3.36	53.7
5 (#3)	9.53	400	200	1000	1692	2.97	57.0
6 (#3)	9.53	400	200	1000	1800	3.21	56.0
Mean					1764	3.18	55.6
7 (#4)	12.7	400	200	1000	1642	3.43	47.9
8 (#4)	12.7	400	200	1000	1605	3.27	49.1
9 (#4)	12.7	400	200	1000	1567	3.21	48.9
Mean					1605	3.30	48.6

170 Note: ∅ is nominal diameter of GFRP reinforcement bar, L_a is steel anchor length, L is free
171 length, L_{tot} is total length of tensile test specimen, f_u is tensile strength, ε_{fu} is rupture strain and
172 E_f is elastic modulus.

173 **2.2 Specimen Design and Preparation**

174 In this study, six beams reinforced with GFRP bars were cast and experimentally tested under
175 three point loading. Three beams were cast with nominal concrete strength of 80 MPa and three
176 beams were cast with nominal concrete strength of 120 MPa. All specimens were 100 mm wide,
177 150 mm high and 2400 mm long. Shear span-to-depth ratio was approximately 8 for all beams.
178 Cross-sectional dimensions and schematic view of the GFRP-RC beams are presented in Fig. 2.
179 All GFRP-RC beams were doubly reinforced, with two GFRP reinforcement bars in the tensile
180 zone and two GFRP reinforcement bars in the compressive zone. It is noted that investigations
181 on the effect of top reinforcement in the compressive zone is beyond the scope of the paper and
182 is considered part of the future research by the authors and research collaborators. Longitudinal
183 GFRP tensile reinforcement ratios were 0.5%, 1.0% and 2.0%. The concrete cover was 15 mm at
184 the top and bottom of the beams and also at the sides of the beams. (from the tensile face of the
185 GFRP RC beams to the outer surface of the steel reinforcement stirrups). Steel reinforcement

was used as shear links with 4 mm diameter bar and spaced evenly at 50 mm centres to ensure that beams were flexural-critical.

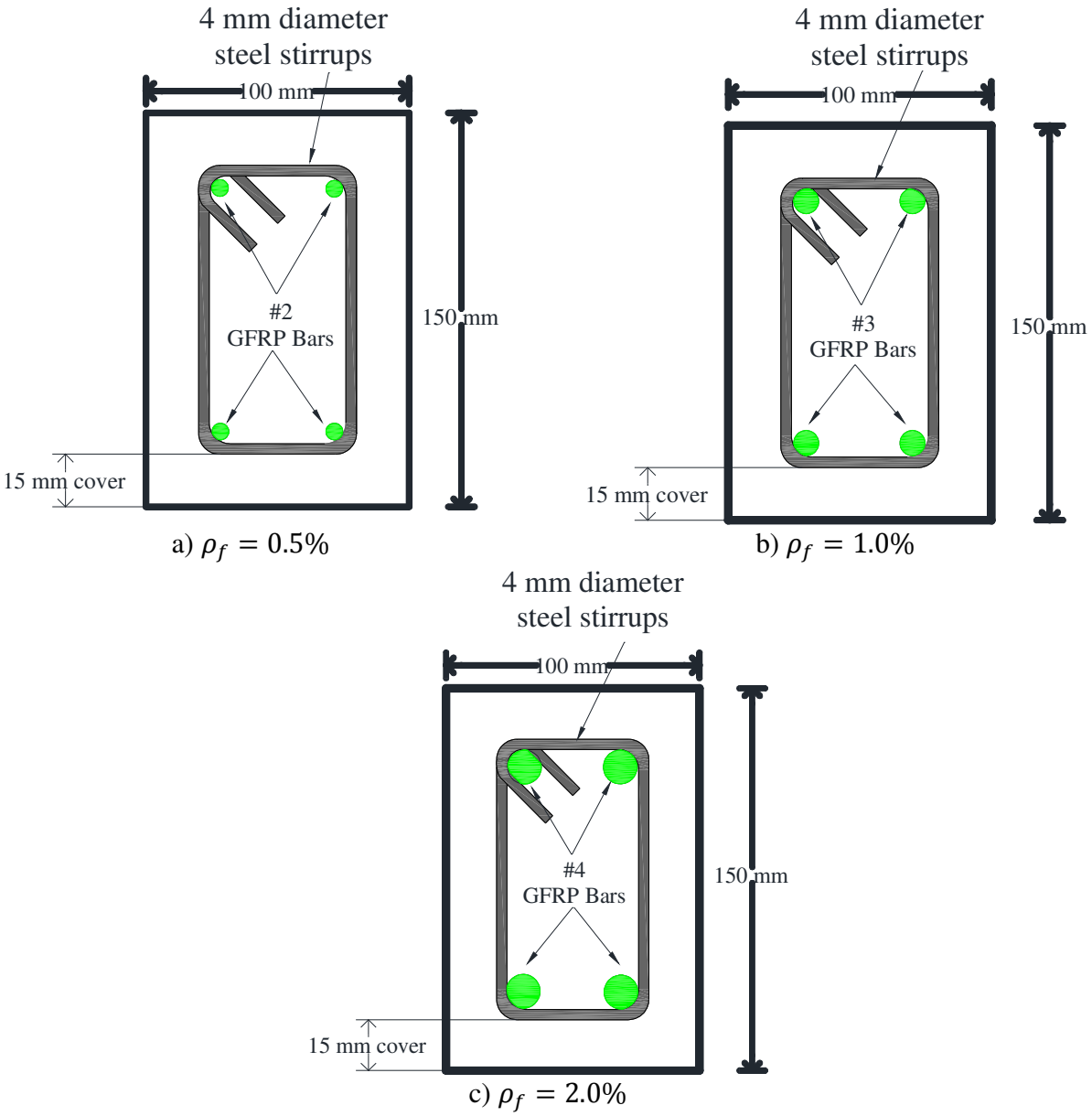

Fig. 2. Cross-Section of GFRP-RC Beams

Beams with a tensile longitudinal reinforcement ratio of $\rho_f = 0.5\%$ were under-reinforced (GFRP reinforcement rupture governs) and beams with a tensile longitudinal reinforcement ratio

of $\rho_f = 1.0\%$ and 2.0% were over-reinforced (concrete crushing governs). Nominal load capacities (P_n) were computed using the design recommendations for FRP-RC beams [21-22]. Nominal load capacities (P_n) were calculated using experimental data from preliminary material testing results. GFRP-RC beams were classified in the form A-B-C, where A represents the nominal concrete strength, B represents the type of GFRP reinforcement bar and C represents the reinforcement ratio. For example, GFRP-RC beam 120-#3-1.0 was designed to have nominal concrete strength of 120 MPa, #3 GFRP reinforcement bars and a tensile longitudinal reinforcement ratio of $\rho_f = 1.0\%$. Table 3 reports the reinforcement details of the GFRP-RC beams.

Table 3. Details of GFRP-RC Beams

GFRP-RC Beam	ρ_f (%)	Bottom Reinforcements (GFRP Bars)	Nominal Moment Capacities, M_n (kNm)		Design Failure Mode
			(ACI 2015)	(CSA 2012)	
80-#2-0.5	0.5	2×#2	5.7	5.8	GFRP Rupture
80-#3-1.0	1.0	2×#3	13.6	13.9	Concrete Crushing
80-#4-2.0	2.0	2×#4	16.0	15.5	Concrete Crushing
120-#2-0.5	0.5	2×#2	5.7	5.8	GFRP Rupture
120-#3-1.0	1.0	2×#3	15.2	14.6	Concrete Crushing
120-#4-2.0	2.0	2×#4	18.0	17.2	Concrete Crushing

where: ρ_f is FRP reinforcement ratio and M_n is nominal moment capacity.

209 **2.3 Testing Procedure**

210 The GFRP-RC beams were simply supported and tested under three point loading (Fig. 3).
211 Effective span of the beams was 2000 mm, with a shear span of 1000 mm and overhang of 200
212 mm on each side. Each GFRP-RC beam was supported with a pin and a roller at the ends,
213 allowing for the beams to deflect under monotonic increasing load. A 600 kN hydraulic actuator
214 anchored to an independent steel frame was used to apply a monotonic increasing load on a steel
215 circular plate at the mid-span. GFRP-RC beams were tested under displacement controlled
216 loading at the rate of 1 mm/min until failure. Two electrical resistance strain gauges were
217 attached at the top on each side of the GFRP-RC beams, directly underneath the position of the
218 load cell to measure concrete strain (Fig. 4). Two strain gauges were attached at the centres of
219 the tensile GFRP reinforcement bars to measure tensile strain. During testing, cracks were
220 marked and the corresponding loads were recorded. All data including load, mid-span deflection
221 and strain were recorded using a high speed data acquisition system.

222

223 **Fig. 3.** Test Setup and Instrumentation

224

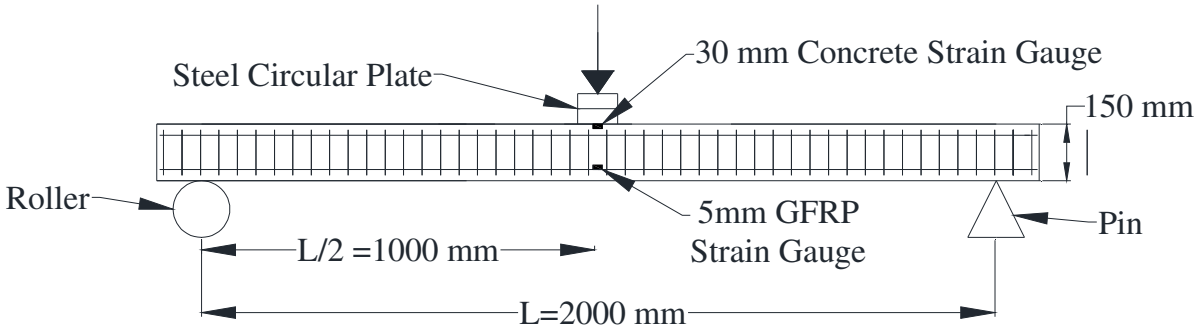

225

226 **Fig. 4.** Schematic View of GFRP-RC beams

227

228

3. Experimental Results and Analysis

3.1 Failure Modes

For the two under-reinforced HSC and UHSC GFRP-RC beams (80-#2-0.5 and 120-#2-0.5), similar crack patterns and identical failure modes were observed. Signs of vertical cracking around the mid-span were evident at a load of 3.1 kN for the HSC GFRP-RC beam (80-#2-0.5) and 3.3 kN for the UHSC GFRP-RC beam (120-#2-0.5). After the formation of flexural cracks around the mid-span, new vertical cracks began propagating closer to the supports as the load increased. During the formation of these new cracks, already formed cracks around the mid-span continued to propagate throughout the height of the HSC and UHSC GFRP-RC beams, close to the compressive zone. Also, the already formed cracks began to widen, right underneath the loading point. At the point of failure, the GFRP reinforcement bars ruptured at the region of maximum bending moment, defined as peak 1 (Fig. 5). This caused the flexural cracks around the mid-span to widen significantly, causing concrete cover to spall off in tension. No prior warning of collapse was evident, with failure occurring in a sudden, brittle manner. Also, concrete on the top surface remained undamaged at the time of failure. This type of failure mode has also been found in the literature, where a tension failure in the FRP reinforcement bars occurred [4, 6, 27-28].

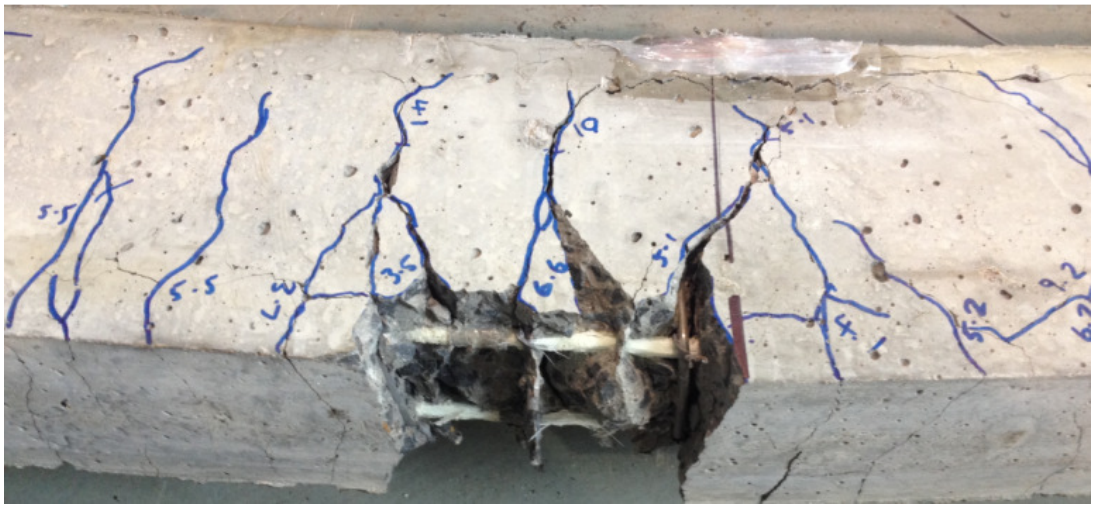

Fig. 5. GFRP Reinforcement Bar Rupture

For the over-reinforced HSC and UHSC GFRP-RC beams (80-#3-1.0, 120-#3-1.0, 80-#4-2.0, 120-#4-2.0), vertical cracks initially formed (at a cracking loads ranging from 3.8 kN to 4.0 kN for HSC and 3.0 kN to 3.5 kN for UHSC) around the mid-span region and continued to branch closer towards the support regions. The average spacing of the major flexural cracks formed was measured as approximately 50 mm. As the load increased, the formation of flexure-shear cracks were evident closer to the supports. During the formation of the flexure-shear cracks, concrete crushing of the cover on the top surface was noticed and crushed initally on one side of the loading point. At this loading stage, a drop in load carrying capacity was evident, defined as peak 1 (Fig. 6 (a)). The load at peak 1 for the over-reinforced HSC GFRP-RC beams ranged from 33.0 kN to 46.1 kN. For the over-reinforced UHSC GFRP-RC beams, load at peak 1 ranged from 41.8 kN to 52.2 kN. This peak (peak 1) was considered "failure", and classifed as the ultimate load carrying capacity (P_u) from a design point of view, due to crushing of concrete cover.

At higher loading stages, after crushing of concrete cover (peak 1), the over-reinforced GFRP-RC beams were able to sustain and carry additional load (reserve capacity or pseudo "ductility").

The rate of formation of new cracks significantly decreased. The majority of already formed flexure and flexure-shear cracks continued to slowly propagate. The next noticable change in the GFRP-RC beams behaviour was additional crushing of concrete cover which occured on the other side of the loading point (peak 2) (Fig. 6 (b)). The crushing of concrete cover resulted in another major drop in load carrying capacity (peak 2). The load at peak 2 ranged from 44.6 kN to 54.2 kN for the HSC GFRP-RC beams (80-#3-1.0 and 80-#4-2.0). The load at peak 2 ranged from 46.7 kN to 63.1 kN for the UHSC GFRP-RC beams (120-#3-1.0 and 120-#4-2.0). Following the additional crushing of concrete cover (peak 2), the HSC and UHSC GFRP-RC beams still showed signs of reserve capacity, with another increase in load until total failure (peak 3). From peak 2 to peak 3, signs the tensile GFRP reinforcement bars reaching their rupture strain were evident by the formation of cracks along the tensile region around the mid-span. At peak 3, the over-reinforced HSC and UHSC GFRP-RC beams failed due to the rupture and splitting of fibres of the GFRP reinforcement bars as shown in Fig. 6 (c). At peak 3, load ranged from 42.3 kN to 67.1 kN for the over-reinforced HSC GFRP-RC beams. For the UHSC GFRP-RC beams, load at peak 3 ranged from 46.6 kN to 70.3 kN. The rupture of the GFRP reinforcement bars caused the tensile concrete cover to spall off, resulting in widening of existing cracks. Thus the over-reinforced HSC and UHSC GFRP-RC beams displayed two types of failure modes: (a) initially crushing of concrete cover and (b) rupture of the GFRP reinforcement bars.

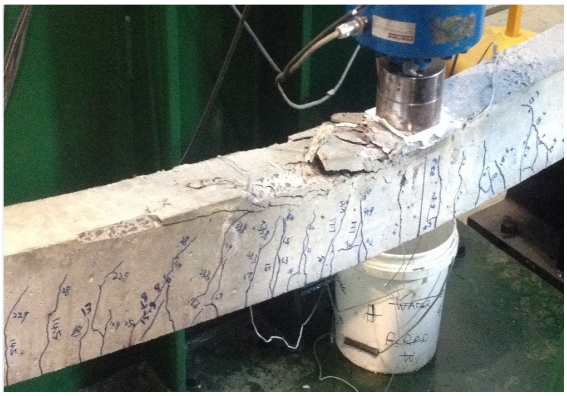

(a) Peak 1 – Initial Concrete Crushing

(b) Peak 2 – Additional Concrete Crushing of Cover

(c) Peak 3 – GFRP Reinforcement Bar Rupture

Fig. 6. Failure of Over-Reinforced GFRP-RC Beam

281

282 **3.2 Load-Midspan Deflection Behaviour**

283 The experimental load-midspan deflection behaviour for the GFRP-RC beams is presented in
284 Fig. 7. The GFRP-RC beams showed a bi-linear behaviour (pre- and post-cracking behaviour) up
285 until total failure. Bi-linear behaviour was also reported for FRP-RC beams under static loading
286 in Ref. [5-7, 12]. Kalpana and Subramanian [12] reported that GFRP-RC beams under static
287 loading showed a linear-elastic behaviour up to failure. For the two under-reinforced HSC and
288 UHSC GFRP-RC beams (80-#2-0.5 and 120-#2-0.5), failure occurred due to the rupture of the
289 GFRP reinforcement bars without any sign of reserve capacity. However, for the over-reinforced
290 HSC and UHSC GFRP-RC beams (80-#3-1.0, 120-#3-1.0, 80-#4-2.0, 120-#4-2.0), some amount
291 of pseudo "ductility" was observed. Fig. 8(a) and Fig 8(b) explains the behaviour of the GFRP-

RC beams at various loading levels for an over-reinforced and under-reinforced GFRP RC beam, respectively. Energy absorption capacities of the HSC and UHSC GFRP-RC beams were calculated using numerical integration of load-midspan deflection graph. Two energy absorption capacities were calculated: E_1 is the energy capacity up to the initial stages of crushing of concrete cover ($\varepsilon_{cu} = 0.003$) for the four over-reinforced HSC and UHSC GFRP-RC beams or failure for the two under-reinforced HSC and UHSC GFRP-RC beams (peak 1); and E_2 is the reserve capacity for the over-reinforced HSC and UHSC GFRP-RC beams (peak 1 to peak 3). Fig. 9 shows an example calculation of the energy absorption capacity (E_1 and E_2).

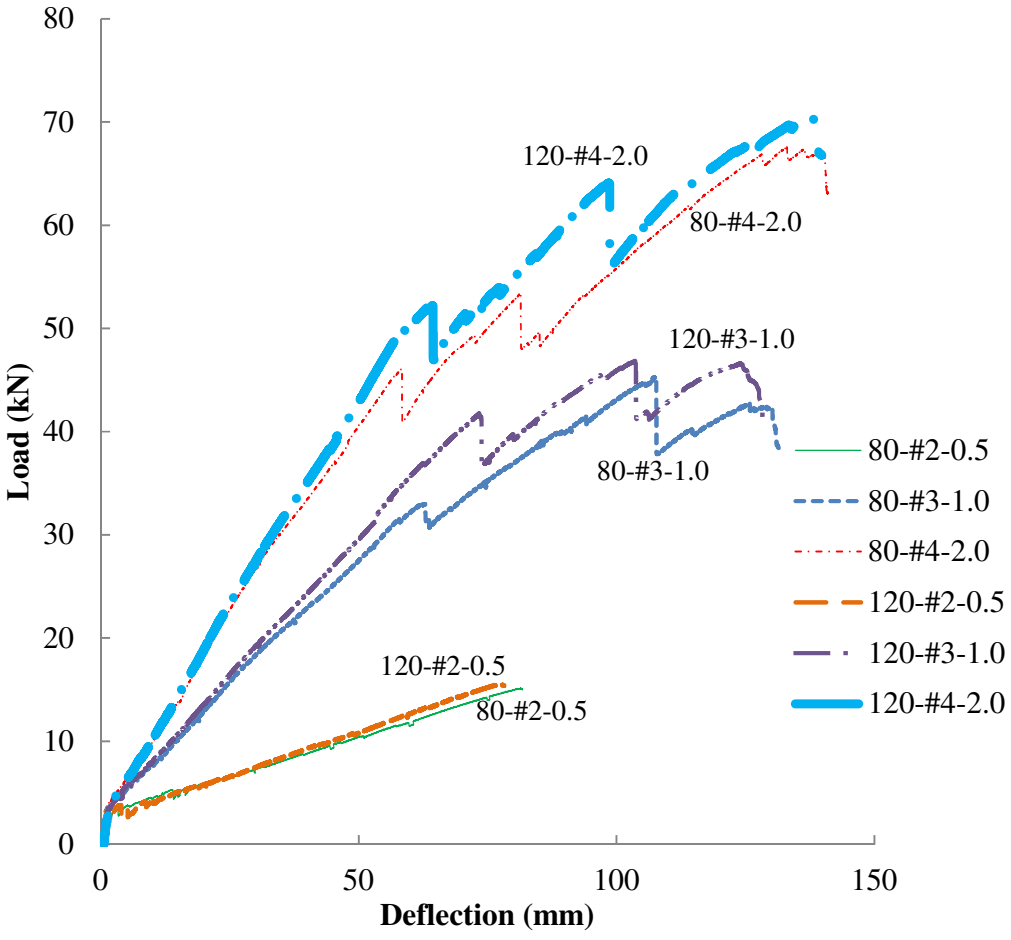

Fig. 7. Load-Midspan Deflection Behaviour of GFRP-RC Beams under Static Loading

302

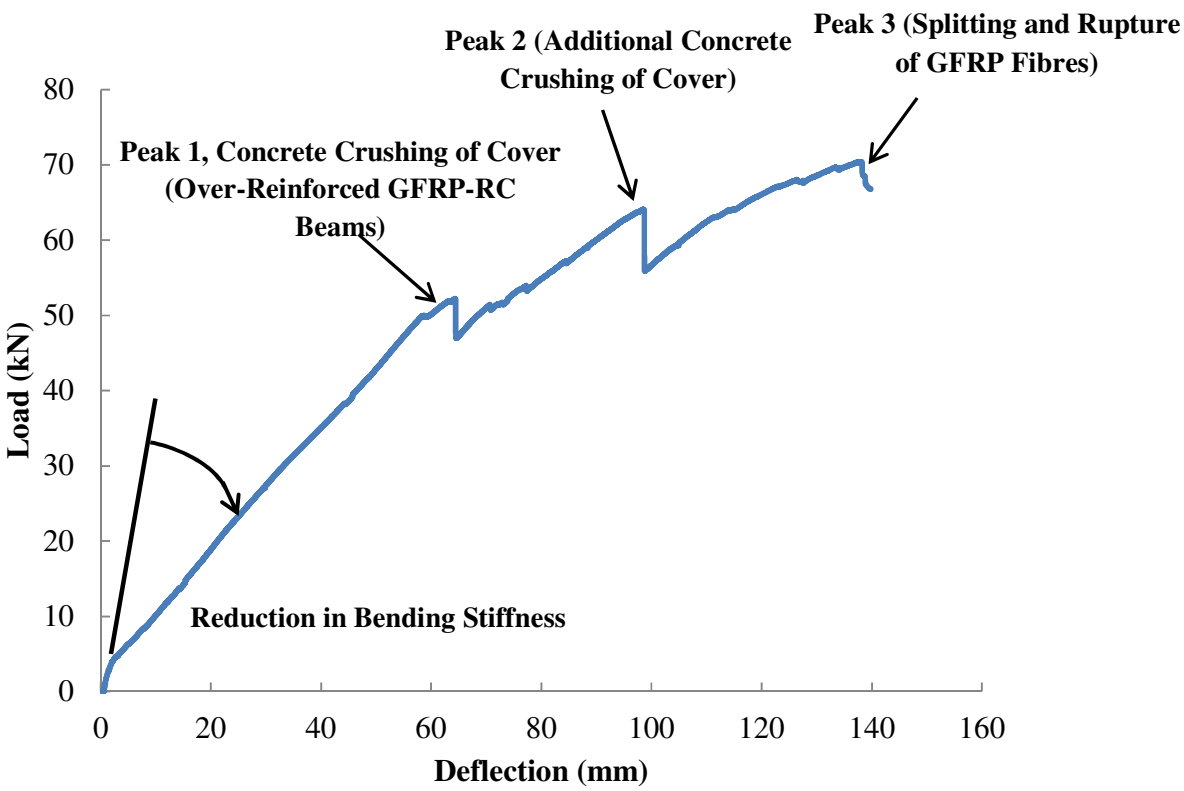

303

304 (a) Over-Reinforced GFRP-RC Beam

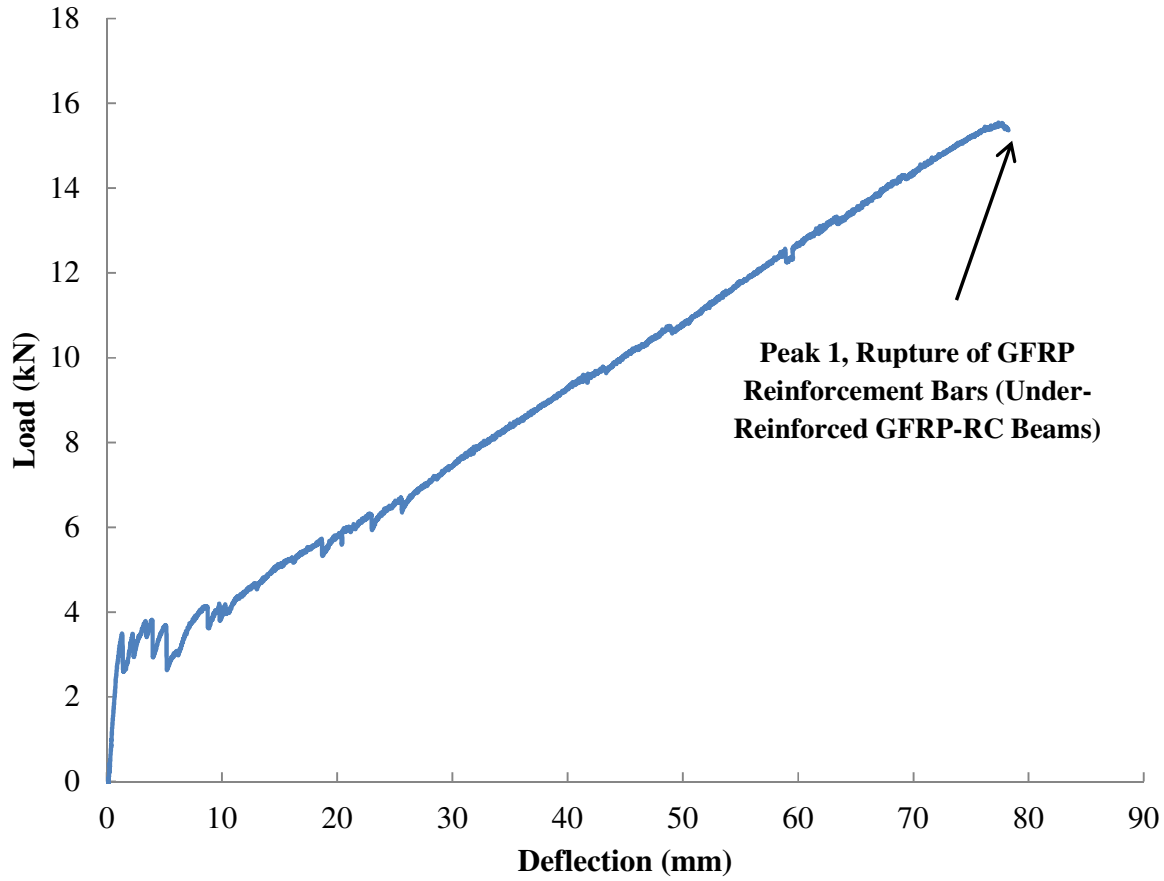

305

306 (b) Under-Reinforced GFRP-RC Beam

307 **Fig. 8.** Definition of Peak Loads in the Behaviour of GFRP-RC Beams under Static Loading

308

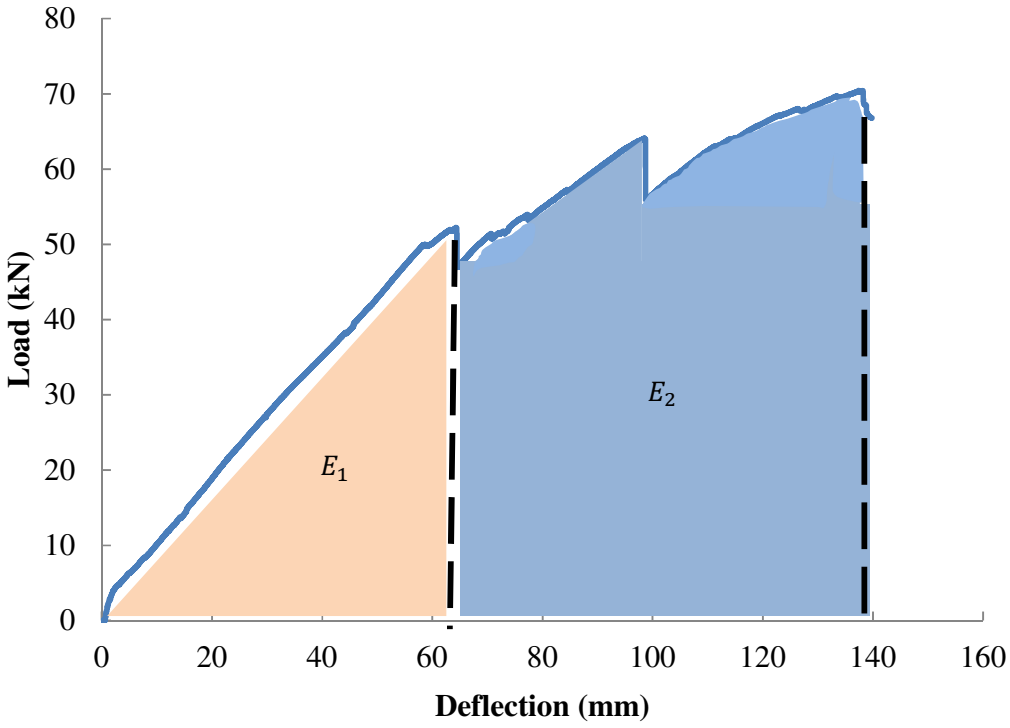

Fig. 9. Energy Absorption Capacity (E_1 and E_2)

3.3 Load-GFRP Strain Behaviour

The load-strain behaviour in the GFRP reinforcement bars is shown in Fig 10. A sudden drop in strain was noticed at the point of cracking. The rapid increase of average post-cracking strain in the GFRP reinforcement bars ($\boldsymbol{\varepsilon_{frp.avg}}$) was found to be dependent on the amount of reinforcement. For the under-reinforced HSC and UHSC GFRP-RC beams (80-#2-0.5 and 120-#2-0.5), average strain in the #2S GFRP reinforcement bars rapidly increased compared to the over-reinforced HSC and UHSC GFRP-RC beams (80-#3-1.0, 120-#3-1.0, 80-#4-2.0, 120-#4-2.0) with #3HM and #4HM GFRP reinforcement bars. Also, concrete strength did not significantly affect strain in GFRP reinforcement bars. UHSC GFRP-RC beams displayed slightly lower strains at the same load level compared to the HSC GFRP-RC beams. The average

strain in the GFRP reinforcement bars at peak 1 could not be established for the six HSC and UHSC GFRP-RC beams since strain gauges were damaged. Thus, linear regression was done up to peak 1, assuming post cracking strain remained linear. Average strain in the GFRP reinforcement bars at peak 1 was shown to vary between 1.3%-1.6% for the over-reinforced HSC GFRP-RC beams (80-#3-1.0 and 80-#4-2.0) and 1.6%-1.9% for the over-reinforced UHSC GFRP-RC beams (120-#3-1.0 and 120-#4-2.0). For the four over-reinforced HSC and UHSC GFRP-RC beams, average strain in GFRP reinforcement at peak 1 was lower than the rupture strain from preliminary material testing, indicating a concrete crushing failure. However, average GFRP reinforcement strain at the point of GFRP reinforcement rupture was calculated as 2.8% for the under-reinforced HSC GFRP-RC beam (80-#2-0.5) and 3.5% for the under-reinforced UHSC GFRP-RC beam (120-#2-0.5). This was much higher than the average rupture strain of 1.96% obtained from preliminary material testing for #2 GFRP reinforcement bars.

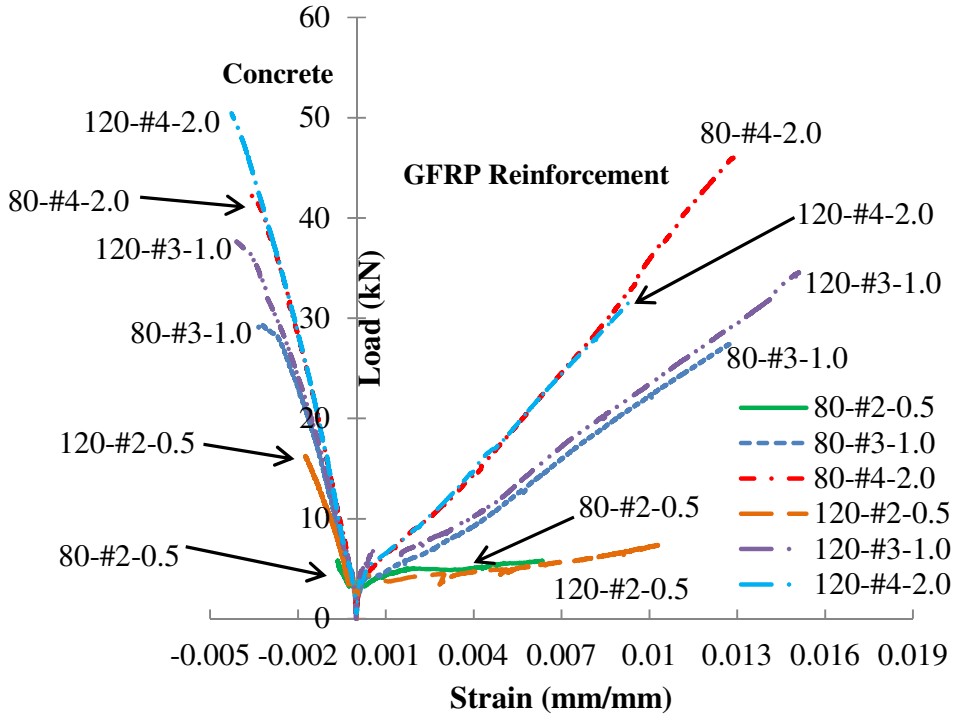

Fig. 10. Load-Strain Behaviour of GFRP-RC Beams under Static Loading

3.4 Load-Concrete Strain Behaviour

Fig. 10 shows the load-strain behaviour for concrete ($\varepsilon_{c.avg}$) for the HSC and UHSC GFRP-RC beams. Using linear regression analysis up to peak 1 (crushing of concrete cover), average concrete strain found to vary between 0.003-0.0035 for the over-reinforced HSC GFRP-RC beams (80-#3-1.0 and 80-#4-2.0). Similarly, for the two over-reinforced UHSC GFRP-RC beams (120-#3-1.0 and 120-#4-2.0) concrete stain at peak 1 was found to be 0.004. This is quite consistent with the assumed maximum compressive strain values of 0.003 and 0.0035 in ACI [21] and CSA [22], respectively. For the under-reinforced HSC and UHSC GFRP-RC beams, average concrete strain at failure was found to be lower than 0.003. For the under-reinforced HSC GFRP-RC beam (80-#2S-0.5), $\varepsilon_{c.avg} = 0.002$ and for UHSC GFRP-RC beam 120-#2-0.5,

$\varepsilon_{c.avg} = 0.0017$, indicating a GFRP reinforcement rupture failure since the assumed maximum compressive strain ($\varepsilon_{cu} = 0.003$ or $\varepsilon_{cu} = 0.0035$) was not attained. Linear regression was not required for determining average concrete strain for the two under-reinforced HSC and UHSC GFRP-RC beams. Finally, increasing concrete strength HSC (95 MPa) to UHSC (117 MPa) showed to have very little effect on concrete strain at the same loading level for all GFRP-RC beams. Table 4 reports the experimental results for the HSC and UHSC GFRP-RC beams under static loading.

Table 4. Experimental Results for GFRP-RC Beams

GFRP-RC Beam (Failure Mode)	Cracking Load, P_{cr} (kN)	Experimental Load Carrying Capacity, P_u (kN)	Mid-span Deflection, Δ_{exp} (mm)	Total Energy Absorption ($E_1 + E_2$) (J)	Average Strain	
					$\varepsilon_{frp.avg}$ (%)	$\varepsilon_{c.avg}$
80-#2-0.5 (GFRP Rupture)	3.1	15.0	81.8	742	2.8*	-0.002
80-#3-1.0 (Concrete Crushing)	3.8	33.0	62.6	3909	1.6*	-0.003*
80-#4-2.0 (Concrete Crushing)	4.0	46.1	58.3	6050	1.3*	-0.0035*
120-#2-0.5 (GFRP Rupture)	3.3	16.2	77.5	714	3.5*	-0.0017
120-#3-1.0 (Concrete Crushing)	3.5	41.8	73.3	4057	1.9*	-0.004*
120-#4-2.0 (Concrete Crushing)	3.0	52.2	64.3	6377	1.6*	-0.004*

Note: * Data was extrapolated using linear regression analysis to calculate average strain at Peak 1

3.5 Influence of Reinforcement Ratio

Increasing the amount of tensile reinforcement showed to enhance the performance of the GFRP-RC beams under static loading. Ashour and Habeeb [27] also reported that increasing tensile reinforcement is key to enhancing load carrying capacity and controlling deflection of simply supported beams. In comparison, Adam et al. [6] reported that by increasing reinforcement ratio

363 from 0.98% to 2.5%, ultimate capacity increased from 132.7 kN to 145.1 kN (increase of 9%) for
364 concrete strength of 70 MPa. This was also verified through experimental results that showed an
365 increase in load carrying capacity (Fig. 11) and reduction in mid-span deflection (Fig. 12) for an
366 increase in the amount of tensile reinforcement. Also, bending stiffness (Fig. 13) and energy
367 absorption capacity significantly increased by increasing reinforcement ratio (Fig. 14).

368

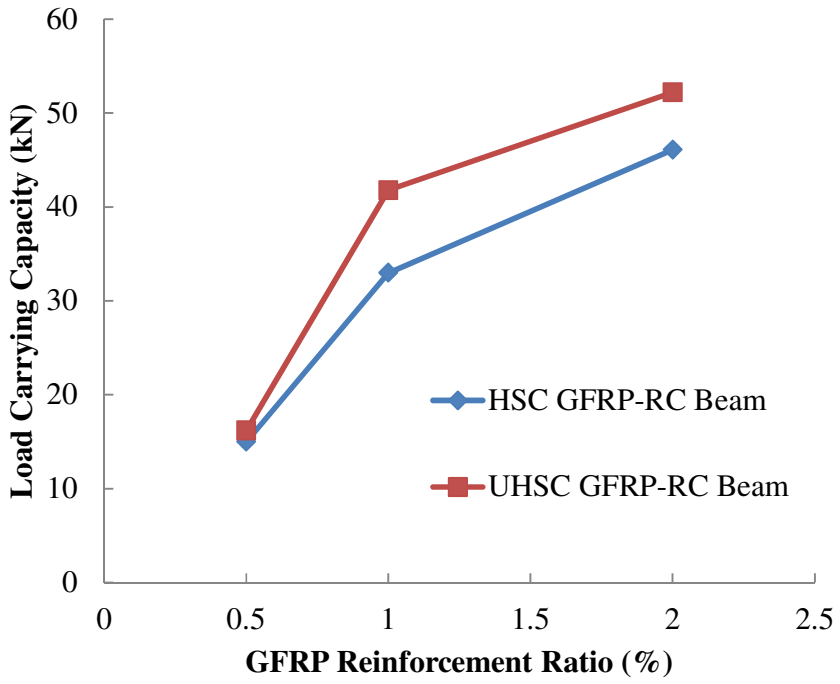

369

370 **Fig. 11.** Effect of Reinforcement Ratio and Concrete Strength on Load Carrying Capacity at
371 Peak 1

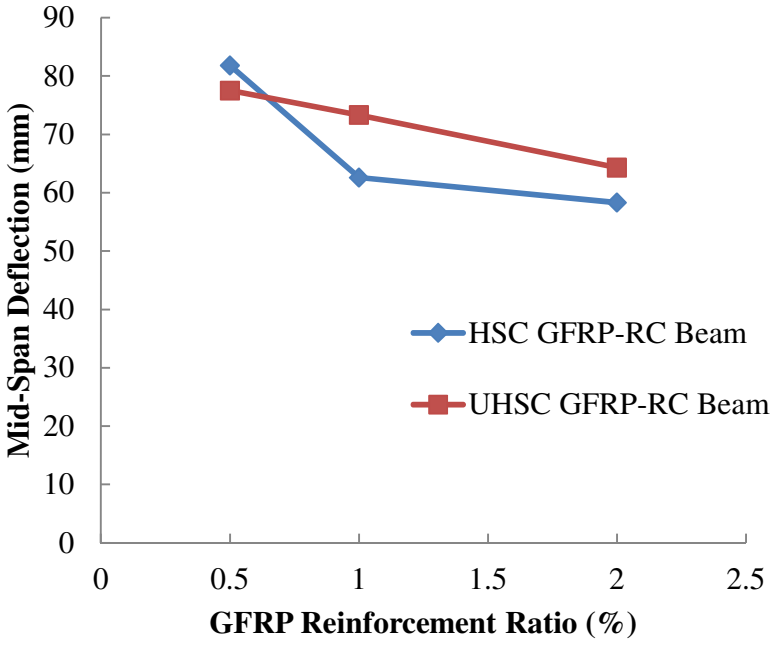

372

373 **Fig. 12.** Effect of Reinforcement Ratio and Concrete Strength on Mid-span Deflection at Peak 1
374 Load

375

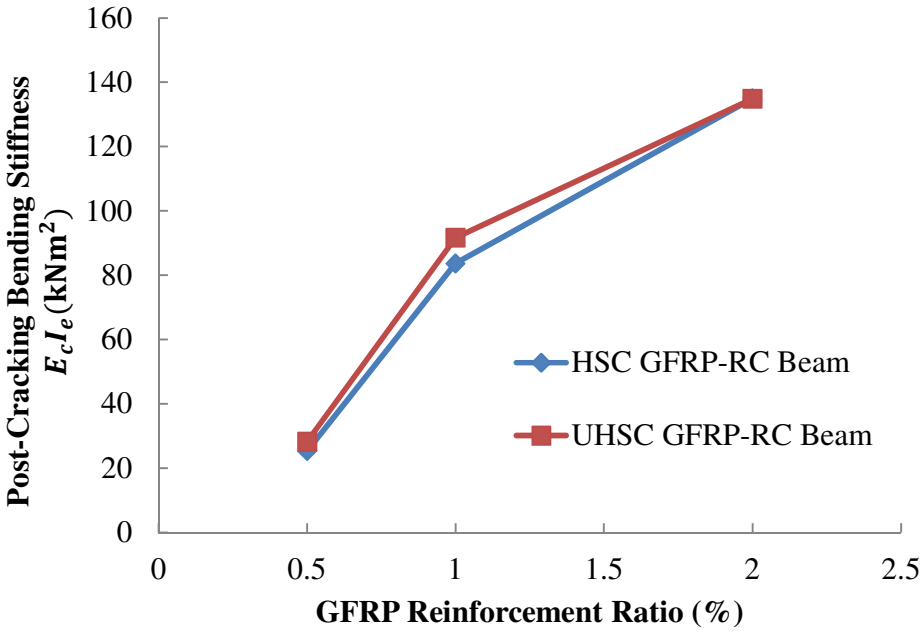

376

377 **Fig. 13.** Effect of Concrete Strength and GFRP Reinforcement Ratio on Post-Cracking Bending
378 Stiffness

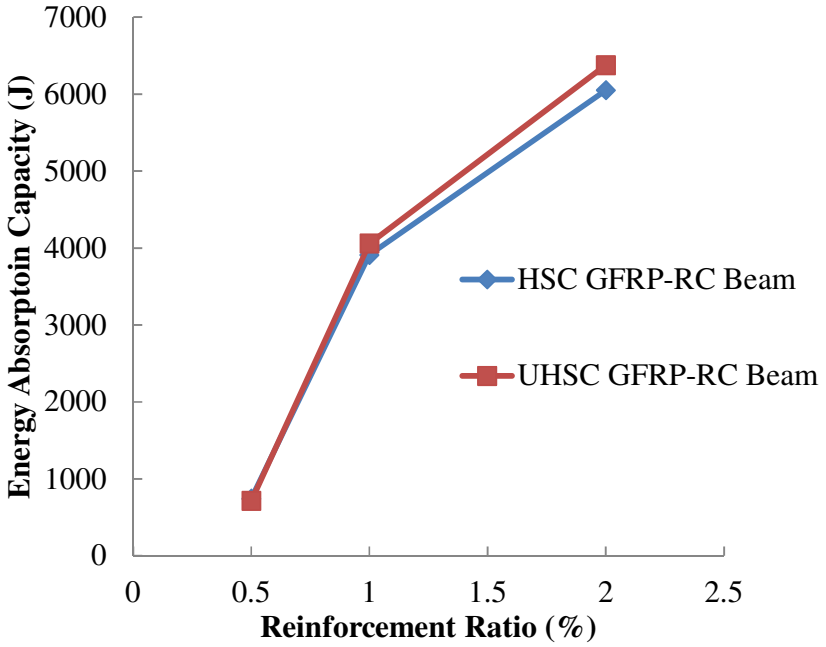

Fig. 14. Effect of Concrete Strength and GFRP Reinforcement Ratio on Energy Absorption Capacity

For an increase in reinforcement ratio from $\rho_f = 0.5\%$ to $\rho_f = 1.0\%$, for the HSC GFRP-RC beams (80-#2-0.5 and 80-#3-1.0), load carrying capacity showed to increase by 120% (from 15 kN to 33 kN) with a reduction in mid-span deflection of 23% (from 81.8 mm to 62.6 mm). Bending stiffness and energy absorption capacities were approximately three and five times higher, respectively. This was also evident for an increase in reinforcement ratio from $\rho_f = 0.5\%$ to $\rho_f = 2.0\%$ (HSC GFRP-RC beams 80-#2-0.5 and 80-#4-2.0) where load carrying capacity increased significantly (207% increase with a reduction in mid-span deflection of 29%). Bending stiffness and energy absorption capacity were found to be approximately 5 and 8 times higher, respectively, for the four times of the amount of tensile reinforcement. The reason for the significantly large percentage increases in load carrying capacity, energy absorption capacity and bending stiffness is attributed to the change in failure mode: from GFRP reinforcement rupture to concrete crushing. However, by increasing the reinforcement ratio from $\rho_f = 1.0\%$ to $\rho_f =$

2.0%, load carrying capacity increased by 40%, with a 7% reduction in the mid-span deflection. Post-cracking bending stiffness increased by 61%. Energy absorption capacity was found to be 1.5 times larger for $\rho_f = 2.0\%$. Similar outcomes were observed for UHSC GFRP-RC beams. For example, by increasing reinforcement ratio from $\rho_f = 1.0\%$ to $\rho_f = 2.0\%$ (UHSC GFRP-RC beams 120-#3-1.0 and 120-#4-2.0), load increased 25%, with a reduction in mid-span deflection of 12%. Furthermore, flexural stiffness and energy absorption capacity increased by approximately 50%.

3.6 Influence of HSC and UHSC

The effect of concrete strength was investigated in terms of load carrying capacity, mid-span deflection, post-cracking bending stiffness and energy absorption capacity. For the HSC and UHSC GFRP-RC beams with $\rho_f = 0.5\%$, the effect of concrete strength showed to have minimal influence on all parameters investigated. By increasing the concrete strength from HSC (95 MPa) to UHSC (117 MPa), load carrying capacity increased by 8% (from 15 kN to 16.2 kN). The reason for the small increase in load carrying capacity was that the HSC and UHSC GFRP-RC beams were designed as under-reinforced and thus the failure was governed by the tensile strength of the GFRP reinforcement bars. Mid-span deflection decreased by 5% (from 81.8 mm to 77.5 mm) with post-cracking bending stiffness increasing 12% (from 25.3 kNm^2 to 28.3 kNm^2) for the increase in concrete strength from 95 MPa (HSC) to 117 MPa (UHSC). El-Nemr et al. [7] and Goldston et al. [5] also reported increases in the flexural stiffness for HSC GFRP-RC beams compared to normal strength concrete GFRP-RC beams. Energy absorption capacities of the GFRP-RC beams were not affected by increase in concrete strength from HSC (95 MPa) to UHSC (117 MPa). GFRP-RC beam 80-#2-0.5 had a capacity of 742 J, compared to 714 J for GFRP-RC beam 120-#2-0.5.

In contrast, concrete strength had more influence on the behaviour of the over-reinforced HSC and UHSC GFRP-RC beams ($\rho_f = 1.0\%$ and $\rho_f = 2.0\%$). This is because the failure was governed by the strength of the concrete. For GFRP-RC beams with $\rho_f = 1.0\%$ and $\rho_f = 2.0\%$, by analysing the behaviour at peak 1, load carrying capacity increased by 27% (from 33 kN to 41.8 kN) and 13% (from 46.1 kN to 52.2 kN), respectively, by increasing concrete strength from HSC (95 MPa) to UHSC (117 MPa). However, increase in the concrete strength from HSC (95 MPa) to UHSC (117 MPa) showed to increase the mid-span deflection for $\rho_f = 1.0\%$ and $\rho_f = 2.0\%$, by 17% and 10%, respectively. Concrete strength had little influence on post-cracking bending stiffness. For the HSC and UHSC GFRP RC beams with a reinforcement ratio of $\rho_f = 1.0\%$ (80-#3-1.0 and 120-#3-1.0) post-cracking bending stiffness increased 10%. For the HSC and UHSC GFRP-RC beams with $\rho_f = 2.0\%$ (80-#4-2.0 and 120-#4-2.0), post-cracking bending stiffness was similar ($E_c I_e = 135$ kNm^2 for both GFRP-RC beams 80-#4-2.0 and 120-#4-2.0), regardless of concrete strength. Also, UHSC (117 MPa) showed to slightly increase energy absorption capacity ($E_1 + E_2$). Increase in concrete strength from HSC (95 MPa) to UHSC (117 MPa) for GFRP-RC beams with $\rho_f = 1.0\%$ and $\rho_f = 2.0\%$ increased energy absorption capacity by 4% and 5%, respectively.

4. Experimental Results versus Code Recommendations

Experimental test data were compared with FRP design recommendations [21-22]. According to ACI [21], there is no upper limit of concrete strength specified. The factor β_1 in ACI [21] is taken as 0.85 for concrete strength up to and including 28 MPa and for concrete strength above 28 MPa, β_1 is reduced continuously at a rate of 0.05 per each of strength in excess of 28 MPa, but not taken less than 0.65. The β_1 of 0.65 is representative of concrete strength greater than or

439 equal to 56 MPa. It is noted that the $\beta_1 = 0.65$ was used for concrete strengths of both HSC (95
440 MPa) and UHSC (117 MPa) for calculation of nominal moment capacities in this study. The
441 CSA [22] doesn't include concrete strength above 80 MPa. Hence, the comparison presented in
442 this study should be evaluated with caution. Nonetheless, the study provides important data for
443 the next generation design recommendations of FRP-RC beams with HSC and UHSC.

444 Nominal load capacities (P_n) from ACI [21] and CSA [22] were calculated for comparison with
445 experimental loading carrying capacities (P_u) using $P_n = 4M_n/L$ for three point loading, where
446 M_n is the nominal moment capacity and L is the clear span length ($L = 2000$ mm). Nominal
447 load capacities were calculated based on the preliminary material testing results. Overall (for
448 both HSC and UHSC GFRP-RC beams), the FRP design recommendations provided relatively
449 conservative results compared to experimental results, with a mean reading of $P_n/P_u = 0.73$ for
450 both ACI [21] and CSA [22]. On average, load carrying capacity was under-predicted by 36%
451 for both HSC and UHSC GFRP-RC beams and thus indicates the FRP design recommendations
452 provide highly conservative results. In terms of concrete strength, it was shown that for the
453 UHSC GFRP-RC beams (120-#2-0.5, 120-#3-1.0, 120-#4-2.0) provided more conservative
454 results for the nominal load carrying capacity compared to experimental load carrying capacity
455 for both ACI [21] and CSA [22] compared to the HSC GFRP-RC beams (80-#2-0.5, 80-#3-1.0,
456 80-#4-2.0). According to ACI [21], for the UHSC GFRP-RC beams, a mean value of $P_n/P_u =$
457 0.71 was calculated (under-prediction of load by 41%) compared to $P_n/P_u = 0.76$ for the HSC
458 GFRP-RC beams (under-prediction of load by 32%). Similarly, according to CSA [22], for the
459 UHSC GFRP-RC beams (120-#2-0.5, 120-#3-1.0, 120-#4-2.0), an average of nominal load to
460 experimental load carrying capacity of $P_n/P_u = 0.68$ was obtained, indicating an under-
461 prediction of 47%, compared to 30% for the HSC GFRP-RC beams. In terms of GFRP

462 reinforcement ratio, it was found that the most conservative results occurred at the highest
463 reinforcement ratio ($\rho_f = 2.0\%$). For $\rho_f = 2.0\%$ (HSC and UHSC GFRP-RC beams 80-#4-2.0
464 and 120-#4-2.0), an average of $P_n/P_u = 0.69$ (under-prediction of load by 45%) and $P_n/P_u =$
465 0.68 (under-prediction of load by 47%) were calculated for ACI [21] and CSA [22],
466 respectively. For $\rho_f = 0.5\%$ (HSC and UHSC GFRP-RC beams 80-#2-0.5 and 120-#2-0.5), ACI
467 [21] under-predicted load by a mean of 37%, with the least conservative results coming for a
468 reinforcement ratio of $\rho_f = 1.0\%$ (HSC and UHSC GFRP-RC beams 80-#3-1.0 and 120-#3-
469 1.0), under-prediction of load carrying capacity by a mean of 28%. Similarly, CSA [22] under-
470 predicted load by 39% for $\rho_f = 0.5\%$ and 30% for $\rho_f = 1.0\%$. Table 5 summaries nominal load
471 carrying capacity with experimental load carrying capacity for the HSC and UHSC GFRP-RC
472 beams.

473 **Table 5.** Comparison between Nominal and Experimental Load Carrying Capacities

Beam	**Experimental Load, P_u (kN)**	**Nominal Load, P_n (kN)**		**P_n/P_u**	
		(ACI 2015)	**(CSA 2012)**	**(ACI 2015)**	**(CSA 2012)**
80-#2-0.5	15.0	11.4	11.3	0.76	0.75
80-#3-1.0	33.0	27.1	27.7	0.82	0.84
80-#4-2.0	46.1	32.3	32.7	0.70	0.71
120-#2-0.5	16.2	11.3	11.2	0.70	0.69
120-#3-1.0	41.8	30.5	29.3	0.73	0.70
120-#4-2.0	52.2	36.0	34.5	0.69	0.66
Mean				0.73	0.73

474

475 Experimental load-midspan deflections were compared with load-midspan deflection calculation
476 in ACI [21] and CSA [22]. According to ACI [21], the effective moment of inertia (I_e) used for
477 calculation of cracked FRP-RC beams is shown in Equation (1). Equation (1) includes an
478 integration factor, γ which is based on the loading condition (three point loading, four point

479 loading, uniform distributed load etc.) and boundary conditions (simply supported, fixed etc.).
480 Equation (2) represents the integration factor for three point loading. The integration factor
481 accounts for the stiffness along the FRP-RC beam. According to ACI [21] deflection pre- and
482 post-cracking can be obtained using Equation (3) for three point loading. CSA [22] suggests the
483 moment-curvature relationship for calculation of deflection, which has been shown to be suited
484 for FRP-RC beams [29]. This method does not use an effective moment of inertia equation. This
485 approach uses a tri-linear moment-curvature relationship, with three slope segments, that is pre-
486 cracking ($E_c I_g$), zero slope and post-cracking ($E_c I_{cr}$). Pre-cracking, deflection can be obtained
487 using the empirical formula shown in Equation (3). However, post-cracking, CSA [22] suggests
488 Equation (4) for three point loading.

$$I_e = \frac{I_{cr}}{1 - \gamma \left(\frac{M_{cr}}{M_a}\right)^2 \left[1 - \frac{I_{cr}}{I_g}\right]} \tag{1}$$

489

$$\gamma = 3 - 2\left(\frac{M_{cr}}{M_a}\right) \tag{2}$$

490

$$\delta = \frac{PL^3}{48E_c I} \tag{3}$$

491

$$\delta_{max} = \frac{PL^3}{48E_c I_{cr}} [1 - 8\eta \left(\frac{L_g}{L}\right)^3] \tag{4}$$

492

where: M_a is applied moment, $I_g = bh^3/12$ is gross moment of inertia, b is width of beam, h is height of beam, $M_{cr} = 7 \times \lambda \times \sqrt{f'_c} \times I_g/y_t$ (cracking moment, (ACI [21])), $M_{cr} = f_r \times I_g/y_t$ (cracking moment, (CSA [22])), f_r is modulus of rupture ($f_r = 0.6 \times \lambda \times \sqrt{f'_c}$), y_t is distance from centroidal axis of gross section, neglecting reinforcement, to tension face, λ is modification factor reflecting the reduced mechanical properties of lightweight concrete, taken as 1.0 for this study, f'_c is nominal concrete compressive strength, $I_{cr} = bd^3k^3/3 + n_f A_f d^2(1-k)^2$ (moment of inertia of transformed cracked section), d is effective depth, A_f is area of FRP reinforcement, n_f is the ratio of elastic modulus of FRP bar (E_f) to modulus of elastic of concrete (E_c), $k = \sqrt{2\rho_f n_f + (\rho_f n_f)^2} - \rho_f n_f$ (ratio of depth of neutral axis to reinforcement depth), ρ_f is reinforcement ratio, ρ_{fb} is balanced reinforcement ratio, E_c is elastic modulus of concrete, P is applied load, L is span length, L_g is distance from the support to the point where $M_a = M_{cr}$ in a simply supported beam and $\eta = (1 - I_{cr}/I_g)$.

Deflection obtained from ACI [21] and CSA [22] were compared with experimental deflection at experimental load carrying capacity (P_u). At P_u, according to ACI [21], overall deflection was under-predicted for both the HSC and UHSC GFRP-RC beams by an average of 22% ($\Delta_{pred}/\Delta_{exp} = 0.82$). However, the theoretical load-deflection graph calculated using the effective moment of inertia equation provided by ACI [21] did not match well compared to the experimental load-deflection HSC and UHSC GFRP-RC beams with $\rho_f = 0.5\%$ (80-#2-0.5 and 120-#2-0). For HSC GFRP-RC beam 80-#2S-0.5, $\Delta_{pred}/\Delta_{exp} = 0.7$ and for UHSC GFRP-RC beam 120-#2-0.5, $\Delta_{pred}/\Delta_{exp} = 0.73$. The approach for calculation of deflection according to CSA [22] was shown to be more accurate for all GFRP-RC beams. Overall, CSA [22] under-predicted deflection by an average of 10% ($\Delta_{pred}/\Delta_{exp} = 0.91$) for the HSC and UHSC GFRP-

RC beams. The model provided by CSA [22] showed to accurately predict deflection compared to ACI [21] regardless of reinforcement ratio.

In terms of concrete strength (HSC and UHSC), according to the effective moment of inertia equation in ACI [21] it was found that deflection was under-predicted by an average of 19% ($\Delta_{pred}/\Delta_{exp}= 0.84$) for the UHSC GFRP-RC beams (120-#2S-0.5, 120-#3-1.0 and 120-#4-2.0). However, it was found that deflection was even more un-conservative, with the effective moment of inertia equation in ACI [21] under-predicting deflection by an average of 25% ($\Delta_{pred}/\Delta_{exp}= 0.80$) for the HSC GFRP-RC beams (80-#2S-0.5, 80-#3-1.0 and 80-#4-2.0). In contrast, for the HSC GFRP-RC beams, CSA [22] was found to under-predict deflection by an average of 12% ($\Delta_{pred}/\Delta_{exp}= 0.89$) and only under-predict deflection by an average of 7.5% for the UHSC GFRP-RC beams ($\Delta_{pred}/\Delta_{exp}= 0.93$). Thus, the approach for calculation of deflection provided in CSA [22] and ACI [21] were found to be more accurate with experimental deflection for the UHSC GFRP-RC beams compared to the HSC GFRP-RC beams. However, overall, it was found that the two approaches for calculation of deflection provided un-conservative results compared to the experimental deflection. Table 6 compares the predicted deflections with the experimental deflections. Fig. 15 compares experimental load-deflection behaviour with predicted load-deflection behaviour for all GFRP-RC beams.

536 **Table 6.** Experimental and Predicted Deflections

Beam	Measured Deflection, Δ_{exp} (mm)	Predicted Deflection, Δ_{pred} (mm)		$\Delta_{pred}/\Delta_{exp}$	
		(ACI 2015)	(CSA 2012)	(ACI 2015)	(CSA 2012)
80-#2-0.5	81.8	57.3	72.8	0.70	0.89
80-#3-1.0	62.6	51.3	53.8	0.82	0.86
80-#4-2.0	58.3	51.3	53.6	0.88	0.92
120-#2-0.5	77.5	56.6	73.6	0.73	0.95
120-#3-1.0	73.3	65.2	68.2	0.89	0.93
120-#4-2.0	64.3	57.2	58.5	0.89	0.91
Mean				0.82	0.91

537

538 It was observed that that the calculated nominal load carrying capacity in ACI [21] and CSA [22]
539 is highly conservative compared to experimental load carrying capacity for HSC GFRP-RC and
540 UHSC GFRP-RC beams. It should be noted that the design recommendations in CSA [22] were
541 not developed for concrete compressive strengths more than 80 MPa. Also, stress block
542 parameters in ACI [21] reach limiting values at concrete compressive strength of 56 MPa.
543 Hence, the above observation should not be considered as a limitation of the design
544 recommendations in ACI [21] and CSA [22]. Rather, the observation justifies the need to
545 calibrate stress block parameters for HSC and UHSC GFRP-RC beams.

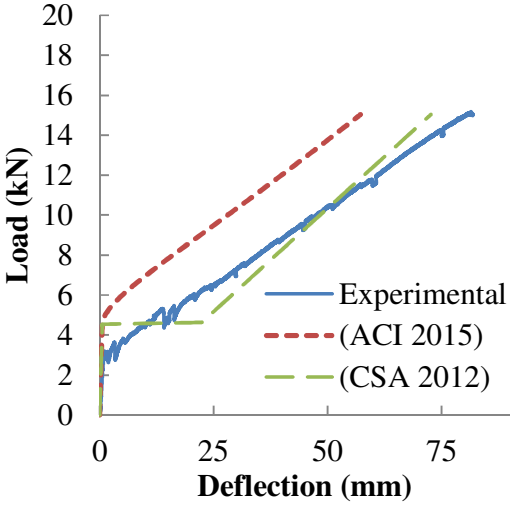

(i) GFRP-RC Beam 80-#2-0.5

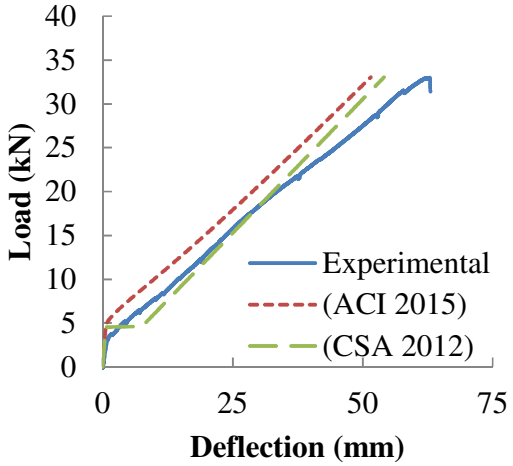

(ii) GFRP-RC Beam 80-#3-1.0

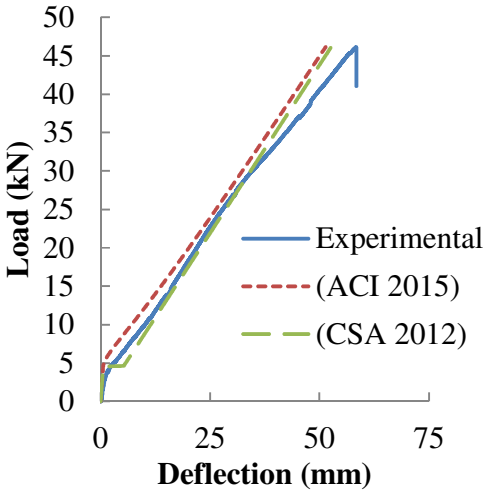

(iii) GFRP-RC Beam 80-#4-2.0

(a) HSC GFRP-RC Beams

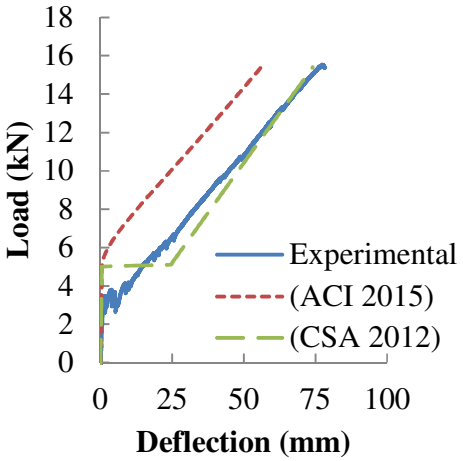

(i) GFRP-RC Beam 120-#2-0.5

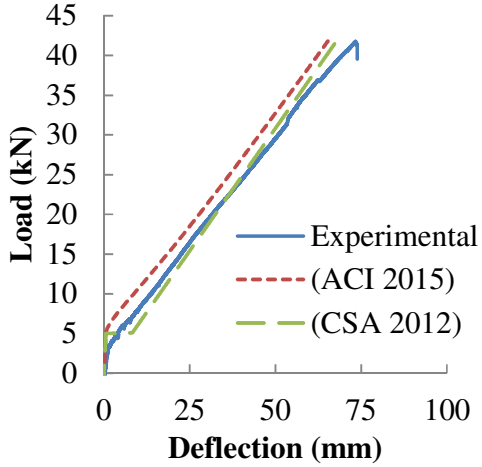

(ii) GFRP-RC Beam 120-#3-1.0

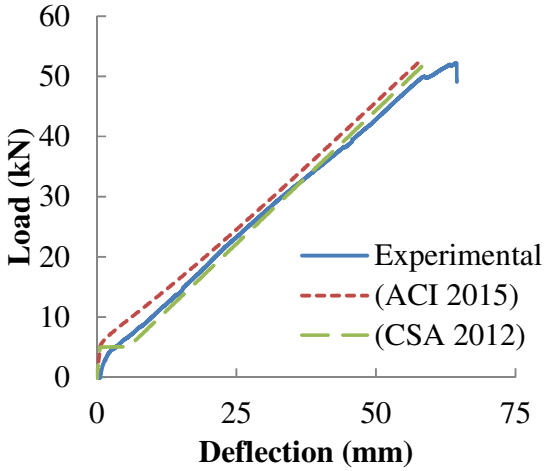

(iii) GFRP-RC Beam 120-#4-2.0

(b) UHSC GFRP-RC Beams

Fig. 15. Comparison of Predicted and Experimental Load-Deflection

5. Conclusions

An experimental program of HSC and UHSC GFRP-RC beams under static loading has been presented. The study investigated the flexural behaviour of HSC and UHSC GFRP-RC beams. Based on the experimental findings, the following conclusions can be drawn:

1. HSC and UHSC GFRP-RC beams displayed a bi-linear relationship up to failure. Regardless of concrete strength (HSC or UHSC), bending stiffness decreased once cracking occurred. The effect of increasing concrete strength from HSC (95 MPa) to UHSC (117 MPa) showed to have little influence on increasing post-cracking bending stiffness for the same amount of longitudinal GFRP reinforcement. Increasing concrete strength from HSC to UHSC showed to increase load carrying capacity more significantly for higher amounts of tensile longitudinal reinforcement ($\geq 1.0\%$). Furthermore, increasing from HSC (95 MPa) to UHSC (117 MPa) showed to have negligible effect on increasing cracking load.

2. HSC and UHSC GFRP-RC beams designed as over-reinforced displayed signs of reserve capacity or pseudo "ductility" compared to the HSC and UHSC under-reinforced GFRP beams where brittle failure occurred. Under-reinforced HSC and UHSC GFRP-RC beams exhibited no reserve capacity. Increasing reinforcement ratio and using UHSC slightly increased the total energy absorption capacity and hence increased reserve capacity or "ductility" of the GFRP-RC beams as opposed to the HSC GFRP-RC beams. For the HSC and UHSC GFRP-RC beams with reinforcement ratios of $\rho_f = 1.0\%$ and $\rho_f = 2.0\%$, total energy absorption capacity increased by 4% and 5%, respectively, for an increase in concrete strength from 95 MPa (HSC) to 117 MPa (UHSC). Increasing

concrete strength from 95 MPa to 117 MPa had no effect on energy absorption capacity for the under-reinforced HSC and UHSC GFRP-RC beams.

3. The GFRP reinforcement bars displayed sharp increases in post-cracking strain for the HSC and UHSC GFRP-RC beams with $\rho_f = 0.5\%$ compared to HSC and UHSC GFRP-RC beams with reinforcement ratios of $\rho_f = 1.0\%$ and $\rho_f = 2.0\%$. This was a result of the very low elastic modulus of the #2 GFRP reinforcement bars, $E_f = 37.5$ GPa from preliminary material testing, compared to $E_f = 55.6$ MPa and $E_f = 48.6$ GPa for the #3 and #4 GFRP reinforcement bars, respectively. Furthermore, post-cracking strain in the GFRP reinforcement bars was unchanged for an increase in concrete strength from 95 MPa (HSC) to 117 MPa (UHSC) with the same amount of reinforcement.

4. It was found that the use of UHSC (117 MPa) was more beneficial in increasing load carrying capacity for the over-reinforced GFRP-RC beams compared to HSC (95 MPa). Load carrying capacity increased 27% and 13% for reinforcement ratios of $\rho_f = 1.0\%$ and $\rho_f = 2.0\%$, respectively, when concrete strength increased from 95 MPa (HSC) to 117 MPa (UHSC). However, mid-span deflection was found to increase as concrete strength increased from 95 MPa (HSC) to 117 MPa (UHSC) for the same amount of reinforcement for the over-reinforced GFRP-RC beams. However, using with HSC (95 MPa) or UHSC (117 MPa) had no significant effect on improving load carrying capacity, mid-span deflection, post-cracking bending stiffness or energy absorption capacity behaviour for the under-reinforced HSC and UHSC GFRP-RC beams, as the failure was governed by GFRP reinforcement rupture.

5. FRP design recommendations, ACI [21] and CSA [23] were found to provide overly conservative results for load carrying capacity of the HSC and UHSC GFRP-RC beams. On average, the ratio of nominal load carrying capacity loads to the experimental load carrying capacity was found to be $P_n/P_u = 0.73$. That is, ACI [21] and CSA [23] under-predicted load by an average of 36%. Both FRP design recommendations were shown to provide similar results in terms of concrete strength HSC (95 MPa) and UHSC (117 MPa). For the HSC GFRP-RC beams, ACI [21] and CSA [22] under-predicted load carrying capacity by 32% and 30%, respectively. The UHSC GFRP-RC beams showed even more conservative calculations of nominal load carrying capacity. For the UHSC GFRP-RC beams, ACI [21] and CSA [22] unpredicted load carrying capacity by 41% and 47%, respectively.
6. At the ultimate load (P_u), it was found that both FRP design recommendations, ACI [21] and CSA [22] were un-conservative for mid-span deflections compared to experimental mid-span deflection for the HSC and UHSC GFRP-RC beams. At the ultimate load, average ratio of predicted deflection to experimental deflection was found to be $\Delta_{pred}/\Delta_{exp}$= 0.82 and $\Delta_{pred}/\Delta_{exp}$= 0.91 for ACI [21] and CSA [22], respectively. Overall, ACI [21] under-predicted deflection by an average of 22% compared to 9% by CSA [22]. For the set of GFRP-RC beams, it was found that the mid-span deflection approach provided in CSA [22] was found to match better with experimental results for both HSC GFRP-RC beams and UHSC GFRP-RC beams. ACI [21] was found to under-predict mid-span deflection by an average of 25% and 19% for the HSC GFRP-RC beams and for the UHSC GFRP-RC beams, respectively. In contrast, CSA [22] only under-predicted mid-span deflection by an average of 12% for HSC GFRP-RC beams

615 and 7.5% for UHSC GFRP-RC beams. Overall, it was found that CSA [22] provided an
616 accurate approach in predicting deflection compared to the experimental deflections, in
617 particular for the UHSC GFRP-RC beams. Further experimental studies are needed to
618 improve the code requirements for the design of GFRP reinforced high strength and ultra
619 high strength concrete beams.

Nomenclature

A_f	area of FRP tensile reinforcement
b	width of beam
d	effective depth
E_1	energy absorption up to peak 1
E_2	reserve capacity of over-reinforced GFRP-RC beams
E_c	elastic modulus of concrete
E_f	elastic modulus of FRP reinforcement
f_r	modulus of rupture
f_u	tensile strength of GFRP reinforcement
f'_c	nominal concrete strength
h	height of beam
I	moment of inertia
I_{cr}	moment of inertia of transformed cracked section
I_e	effective moment of inertia
I_g	gross moment of inertia
I_t	gross moment of inertia
k	ratio of depth of neutral axis to reinforcement depth
L	span length of GFRP-RC beam or free length of the tensile test specimen
L_a	length of steel anchors used for tensile test specimens
L_g	distance from the support to the point where $M_a = M_{cr}$ in a simply supported beam
L_{tot}	total length of tensile test specimen

643 M_a applied moment

644 M_{cr} cracking moment

645 M_n nominal bending moment capacity

646 n_f ratio of elastic modulus of FRP bar to modulus of elastic of concrete

647 P load

648 P_{cr} cracking load

649 P_n nominal load carrying capacity

650 P_u experimental load carrying capacity

651 y_t distance from centroidal axis of gross section, neglecting reinforcement, to
652 tension face

653 α_1 stress block factor

654 β_1 factor taken as 0.85 for concret strength up to and including 28 MPa. Factor is
655 reduced at a rate of 0.05 per each 7 MPa of strength greater than 28 MPa but not
656 taken less than 0.65

657 β_d reduction coefficient used in calculating deflection

658 γ integration factor

659 δ deflection

660 δ_{max} maximum deflection

661 Δ deflection

662 Δ_{exp} experimental deflection

663 Δ_{pred} predicted deflection

664 $\varepsilon_{c.avg}$ average strain in concrete from two strain gauges

665 ε_{cu} assumed ultimate strain in concrete, taken as 0.003 or 0.0034

666	$\varepsilon_{frp.avg}$	average strain of the GFRP strain gauges on tensile reinforcement
667	ε_{fu}	rupture strain of GFRP tensile reinforcement
668	η	$1 - I_{cr}/I_g$
669	λ	modification factor reflecting the reduced mechanical properties of lightweight
670		concrete
671	ρ_f	GFRP longitudinal reinforcement ratio
672	ρ_{fb}	balanced GFRP longitudinal reinforcement ratio
673	$\emptyset$	diameter of GFRP reinforcement bar

674 **References**

675 [1] Sun Z, Yang Y, Qin W, Ren S, Wu G. Experimental study on flexural behavior of concrete
676 beams reinforced by steel-fiber reinforced polymer composite bars. Journal of Reinforced
677 Plastics and Composites 2012; 31(24):1737-45.

678 [2] Issa MS, Metwally IM, Elzeiny SM. Influence of fibers on flexural behavior and ductility of
679 concrete beams reinforced with GFRP rebars. Engineering Structures 2011; 33(5):1754-63.

680 [3] Kamal M, Safaan M, Al-Gazzar M. Ductility of concrete beams reinforced with hybrid FRP
681 rebars. HBRC J, Hous & Build Res Cent 2006; 2(3):1–12.

682 [4] Goldston MW, Remennikov A, Sheikh NM. Experimental investigation of the behaviour of
683 concrete beams reinforced with GFRP bars under static and impact loading. Engineering
684 Structures 2016; 113:220-32.

685 [5] Toutanji HA, Saafi M. Flexural behavior of concrete beams reinforced with glass fiber

686 reinforced polymer (GFRP) bars. ACI Structural Journal 2000; 97(5):712-19.

687 [6] Adam MA, Said, M, Mahmoud, AA, Shanour AS. Analytical and experimental flexural
688 behavior of concrete beams reinforced with glass fiber reinforced polymer bars. Construction
689 and Building Materials 2015; 84(0):354-366.

690 [7] El-Nemr A, Ahmed EA, Brahim B. Flexural behaviour and serviceability of normal- and
691 high-strength concrete beams reinforced with glass fiber-reinforced polymer bars. ACI Structural
692 Journal 2013; 110(06):1077-88

693 [8] Ashour AF. Flexural and shear capacities of concrete beams reinforced with GFRP bars.
694 Construction and Building Materials 2006; 20(10):1005-15.

695 [9] Alsayed SH. Flexural behaviour of concrete beams reinforced with GFRP bars. Cement and
696 Concrete Composites 1998; 20(1):1-11.

697 [10] Lapko A, Urbanski M. Experimental and theoretical analysis of deflections of concrete
698 beams reinforced with basalt rebar. Archives of Civil and Mechanical Engineering 2015;
699 15(1):223-30.

700 [11] Rafi MM, Nadjai A, Ali F. Experimental testing of concrete beams reinforced with carbon
701 FRP bars. Journal of composite materials 2007; 41(22):2657-73.

702 [12] Kalpana VG, Subramanian K. Behavior of concrete beams reinforced with GFRP bars.
703 Journal of Reinforced Plastics and Composites 2011; 30(23):1915-22.

704 [13] Theriault M, Benmokrane B. Effects of FRP reinforcement ratio and concrete strength on
705 flexural behavior of concrete beams. Journal of Composites for Construction 1998; 2(1):7-16.

706 [14] Toutanji H, Deng Y. Deflection and crack-width prediction of concrete beams reinforced
707 with glass FRP rods. Construction and Building Materials 2003;17(1):69-74.

708 [15] Faza SS, GangaRao HVS. Glass FRP reinforcing bars for concrete. Fiber reinforced-plastic
709 (FRP) reinforcement for concrete structures; properties and applications. In: Nanni A, editor.
710 Developments in civil engineering, vol. 42. Elsevier Science Publishers 1993. p. 167 –88.

711 [16] Nanni A. Flexural behavior and design of reinforced concrete using FRP rods. Journal of
712 Structural Engineering 1993b; 119(11):3344-59.

713 [17] Yost JR, Gross S. Flexural design methodology for concrete beams reinforced with fiber-
714 reinforced polymers. ACI Structural Journal 2002; 99(3):308-16.

715 [18] Getzlaf D. An investigation into the flexural behaviour of GFRP reinforced concrete beams.
716 Masters of Applied Science Thesis, University of Toronto, Toronto, Canada; 2012.

717 [19] Vincent T, Ozbakkaloglu T. Influence of concrete strength and confinement method on
718 axial compressive behavior of FRP confined high- and ultra high-strength concrete. Composites
719 Part B: Engineering 2013; 50(X):413-28.

720 [20] Ozbakkaloglu T. Behavior of square and rectangular ultra high-strength concrete-filled FRP
721 tubes under axial compression. Composites Part B: Engineering 2013; 54(X):97-111.

722 [21] ACI Committee 440. Guide for the design and construction of structural concrete reinforced
723 with FRP Bars. Farmington Hills (MI): American Concrete Institute; 2015.

724 [22] CSA Canadian Standards Association. Design and construction of building structures with
725 fibre-reinforced polymers. Ontario, Canada: Canadian Standards Association, S806-12; 2012.

726 [23] Standards Australia. Methods of Testing Concrete - Compressive Strength Tests - Concrete,
727 Mortar and Grout Specimens. Sydney, New South Wales, Australia: Standards Australia, AS
728 1012.9; 2014.

729 [24] V-Rod. Composite reinforcing rods technical data sheet. Largs Bay, SA, Australia; 2012.

730 [25] American Society for Testing and Materials (ASTM). Standard Test Method for Tensile
731 Properties of Fiber Reinforced Polymer Matrix Composite Bars. D7205/ D7205M. West
732 Conshohocken (PA); 2006 (11).

733 [26] American Society for Testing and Materials (ASTM). Standard Testing Methods and
734 Definitions for Mechanical Testing of Steel Products. A370-14. West Conshohocken (PA); 2014.

735 [27] Ashour AF, Habeeb MN. Continuous concrete beams reinforced with CFRP bars. Structures
736 & Buildings 2008; 161(6):349-57.

737 [28] Jaeger LG, Mufti A, Tadros G. The concept of the overall performance factor in
738 rectangular-section reinforced concrete beams. Proceedings of the Third International
739 Symposium on Non-Metallic (FRP) Reinforced for Concrete Structures (FRPRCS-3) 1997;
740 Japan Concrete Institute, Tokyo, Japan, pp. 511-18.

741 [29] Mota C, Alminar S, Svecova D. Critical review of deflection formulas for FRP-RC
742 members. Journal of Composite for Construction 2006; 10(3):183-194.